Theor Chem Acc (2011) 129:313–324
DOI 10.1007/s00214-010-0782-y

REGULAR ARTICLE

Nuclear magnetic resonance parameters in water dimer

Teemu S. Pennanen · Perttu Lantto · Mikko Hakala · Juha Vaara

Received: 6 April 2010 / Accepted: 30 June 2010 / Published online: 15 August 2010

Abstract The changes in the computed nuclear magnetic resonance (NMR) parameters of the water dimer with respect to their monomer values were monitored as the geometry of the dimer was systematically varied. Nuclear magnetic shielding constants, shielding tensor anisotropies, nuclear quadrupole coupling constants and spin–spin coupling constants for the hydrogen bond donor and acceptor molecules were calculated at hybrid density-functional theory level. The dimer geometry was specified through the intermolecular oxygen–oxygen distance R_{OO} and the hydrogen bond angle α. A grid of 120 geometries was selected by systematically varying these two parameters. The other geometrical parameters of the dimer were allowed to relax, keeping the two parameters fixed. As the dimer geometry was varied, all NMR parameters were observed to be smoothly behaving. Characteristic changes as a function of the intermolecular geometry were observed. These include, besides the well-known deshielding of the donor hydrogen shielding constant, also influences on the donor deuterium quadrupole coupling constant, as well as the shielding anisotropy of the donor and acceptor oxygens. We discuss the contributions to the total dimerisation effect from, on the one hand, the dominant direct interaction effect at a fixed geometry and, on the other hand, from the quantitatively relevant indirect, geometric effect. A fundamental ambiguity of this partitioning is demonstrated. By forging the general, smooth trends in all the studied NMR parameters into a specific geometric definition, we find our data to be in agreement with the widely used distance criterion for hydrogen bonding in water, $R_{OO} \leq 3.5$ Å.

Keywords Hydrogen bonding · Nuclear shielding · Quadrupole coupling · Spin–spin coupling · Property surfaces · Density-functional theory · Direct and indirect interaction effects

Dedicated to professor Pekka Pyykkö on the occasion of his 70th birthday and published as part of the Pyykkö Festschrift Issue.

Electronic supplementary material The online version of this article (doi:10.1007/s00214-010-0782-y) contains supplementary material, which is available to authorized users.

T. S. Pennanen (✉) · P. Lantto · J. Vaara
NMR Research Group, Department of Physics, University of Oulu, P.O. Box 3000, 90014 Oulu, Finland
e-mail: teemu.pennanen@oulu.fi

M. Hakala
Department of Physics, University of Helsinki, P.O. Box 64, 00014 Helsinki, Finland

T. S. Pennanen · J. Vaara
Laboratory of Physical Chemistry, Department of Chemistry, University of Helsinki, A.I. Virtasen aukio 1, P.O. Box 55, 00014 Helsinki, Finland

1 Introduction

The local microscopic structure of liquid water has recently attracted a lot of attention. This is mainly due to recent X-ray absorption measurements and their interpretation [1] that challenge the traditional on-average-tetrahedral view on the immediate environment of an individual water molecule in the liquid [2, 3]. Wernet et al. [1] concluded that liquid water is mainly comprised of rings and chains of water molecules where, on average, each molecule has only two strong hydrogen bonds with their neighbours. Since this controversial statement, much effort has been invested in finding out whether these measurements could be interpreted in terms of traditional tetrahedral structural

models [4, 5], or whether the traditional evidence for the tetrahedral view could be re-interpreted to support the non-tetrahedral rings-and-chains model [6].

The water dimer is a basic hydrogen-bonded unit and is of crucial importance in understanding the hydrogen bond network in liquid water [7]. Many studies have been devoted to probe the structure, energetics, and various other properties of the dimer, both theoretically and experimentally [8–12]. Nuclear magnetic resonance (NMR) spectroscopy [13] is an important technique in molecular structure determination, both in the liquid and solid state. The NMR parameters of water are known to be sensitive to both intramolecular rovibrational effects [14–16] and hydrogen bonding with water environment [17, 18] but no direct experimental NMR data on the water dimer exists. The dimeric parameters can be indirectly investigated from gas-to-liquid shifts [17], when interpreted through the pairwise additive approximation [19].

There are many theoretical studies on the NMR parameters in water dimer. Some older papers consider geometry dependence of the nuclear shielding tensor $\boldsymbol{\sigma}$ [20, 21] while more recent studies scrutiny the computational requirements of various NMR parameters at the equilibrium geometry [22–24]. In a recent study, the performance of three density-functional theory (DFT) functionals in predicting the hydrogen bonding effects on NMR shielding constants in $(H_2O)_2$ were tested against high-level ab initio results as a function of geometry [25].

In the present study, we investigate several NMR parameters, the shielding constants σ, shielding anisotropies $\Delta\sigma$, nuclear quadrupole coupling constants (NQCCs) χ, and spin–spin coupling constants J for the donor and acceptor molecules in water dimer, as functions of intermolecular geometry. Changes with respect to the monomer parameters are monitored systematically as functions of two geometrical parameters defining the dimer arrangement, the intermolecular oxygen–oxygen distance R_{OO} and the hydrogen bond angle α. This provides a two-dimensional surface of the properties with respect to these coordinates. We concentrate on the data for nuclei (nuclear pairs for J coupling), for which the most noticeable changes occur. These are usually both the oxygen centres and the hydrogen involved in the hydrogen bond. The numerical data for all cases are supplied in the Electronic Supplementary Information.

Since the NMR parameters are sensitive to the immediate environment of the nuclei, the dimer geometry variations and the associated changes in the NMR parameters suggest a means to formulate an NMR-based hydrogen bond definition. However, the overall smoothness of the property hypersurfaces does not justify an unambiguous criterion, and our outcome resembles closely the widely used geometric criteria [26–28] for hydrogen bonding.

Analysing the impact of dimerisation from another point of view, the total change in an NMR parameter can be divided into direct and geometric parts [29]. The geometric contribution refers to the indirect effect due to the intramolecular geometry change, whereas the direct contribution results from the presence of the neighbour without allowing for the geometric relaxation of the monomers. While the dominating effect is found to result from the direct interaction, the analysis involves a fundamental ambiguity related to the partition into geometric relaxation and direct effects.

2 Theory and computational details

2.1 NMR parameters

Nuclear magnetic shielding is a measure of the modification of the external magnetic field at the site of the nucleus caused by the electron distribution responding to the magnetic field [30]. Thus, shielding carries information about the molecular electronic structure. For isotropic media such as liquid water, rapid tumbling of the molecules averages the shielding tensor so that only the shielding constant, one-third of the trace of the time-averaged shielding tensor, contributes to the spectrum. NMR experiments only determine chemical shifts with respect to a similar nucleus in a reference compound, not the absolute shielding constants.

For isotropic liquids, the peak splitting in the spectrum is caused by indirect nuclear spin–spin coupling, which is an electron-mediated interaction between the magnetic dipoles of the nuclei [31]. Similarly as for shielding, motional averaging reduces the tensor to its isotropic average, the spin–spin coupling constant.

Also of interest in the present work are the anisotropic parameters [13], the anisotropy of the ^{1}H and ^{17}O shielding tensors, as well as the ^{2}D and ^{17}O NQCCs, which affect spectra in anisotropic surroundings such as liquid crystals or the solid state and operate through relaxation processes also in isotropic media [32]. $\Delta\sigma$ manifests itself, e.g., in the chemical shift anisotropy relaxation [33].

Nuclear quadrupole coupling constant describes the interaction between the nuclear electric quadrupole moment (possessed by nuclei with spin $\geq$1) and the electric field gradient tensor at the site of the nucleus [34]. NQCC causes rapid relaxation and can be determined from T_1 relaxation time measurements [35].

2.2 Quantum-chemical calculations

Dimer geometries were obtained by a constrained geometry optimisation, where the distance between the oxygens (R_{OO}) and the hydrogen bond angle, $\alpha = \angle(\mathrm{H1-O1\cdots O2})$,

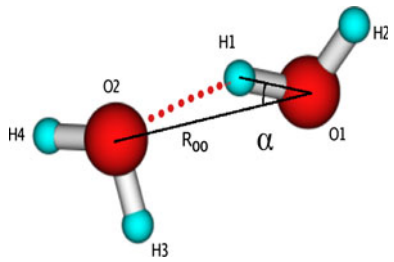

Fig. 1 Geometric parameters and labelling of the nuclei of the water dimer. R_{OO} is the intermolecular oxygen–oxygen distance and $\alpha = \angle(\text{H1-O1}\cdots\text{O2})$ is the hydrogen bond angle

defined in Fig. 1, were kept fixed while the rest of the dimer was allowed to relax. R_{OO} was varied in a systematic manner covering the range of $R_{OO} = 2.5\ldots3.4$ Å in steps of 0.1 Å, as well as 3.6 and 3.8 Å. The angle values were $\alpha = 0$, 5, 10, …, 45°. Altogether, this resulted in 120 dimer geometries. A similar analysis has been recently performed in the context of X-ray Compton scattering [36]. The set of different geometries was chosen to reflect the possible near-neighbour geometries present in liquid water close to normal conditions. The smallest distance ($R_{OO} = 2.5$ Å) is compatible with the appearance of the first signs of neighbours in the oxygen–oxygen radial distribution function [37]. The maximum distance ($R_{OO} = 3.8$ Å) is compatible with the appearance of the second coordination shell with a much weaker interaction than that in the first-shell neighbours. A pair of molecules at this separation is not considered hydrogen bonded. The minimum angle ($\alpha = 0°$) represents a direct hydrogen bond and the maximum angle ($\alpha = 45°$) is dictated by the constrained geometry optimisation (vide infra). Of course, a real instantaneous dimer occurring in the liquid with a pair of values (R_{OO}, α) can have a geometry considerably different from the one found by constrained geometry optimisation. It is assumed, however, that the most probable, minimum-energy structure for a given intermolecular geometry defined by (R_{OO}, α) is representative of those situations as well.

Restricted geometry optimisations were performed at the DFT/B3LYP [38, 39] level using the Gaussian 03 programme [40] with the aug-cc-pVTZ basis set [41, 42], while subsequent NMR property calculations with mostly the DALTON programme [43] used B3LYP with cc-pCVXZ and aug-cc-pCVXZ (X = D, T, Q, 5) basis-set families [41, 44]. Coupled-cluster calculations of NMR properties were carried out using the ACES-II programme [45]. The correlation-consistent basis-set family provides, for both DFT and ab initio calculations, a systematically improving description of the dimerisation-induced changes in mainly the valence region of the electron cloud, where the intermolecular interaction effects principally take place. Shielding calculations used the GIAO ansatz [46, 47] to take care of the gauge problem. Shielding anisotropies, $\Delta\sigma = \sigma_{33} - \frac{1}{2}(\sigma_{11} + \sigma_{22})$, and NQCCs, $\chi = \chi_{33}$, are reported in the principal axis system of the tensors. For $\Delta\sigma$, the principal values are arranged as $\sigma_{11} \leq \sigma_{22} \leq \sigma_{33}$. For the latter property, the principal values are ordered as $|\chi_{11}| \leq |\chi_{22}| \leq |\chi_{33}|$. We report only the differences of the property values between the dimer and monomer, the latter at its calculated equilibrium geometry. In mapping the NMR property surfaces, we do not take into account any rovibrational effects, which would naturally influence the outcome of any experiment on the dimer or condensed-phase systems.

3 Results and discussion

3.1 Test calculations

3.1.1 Basis set and functional selection

Calculations of all the NMR parameters with cc-pCVXZ and aug-cc-pCVXZ basis-set families were performed for the water monomer ($r_{OH} = 0.9618$ Å, $\angle$(H-O-H) = 105.09°) and dimer ($R_{OO} = 2.917$ Å, $\alpha = 5.30°$) at their equilibrium geometries optimised at the B3LYP/aug-cc-pVTZ level. As examples, the basis-set convergence behaviour of the ^{17}O shielding constants and $^{1}J_{O1H1}$ spin–spin coupling constants are shown in Figs. 2 and 3, respectively. The monomer and dimer values along with their difference are displayed. The augmented basis sets display a rapid convergence of the

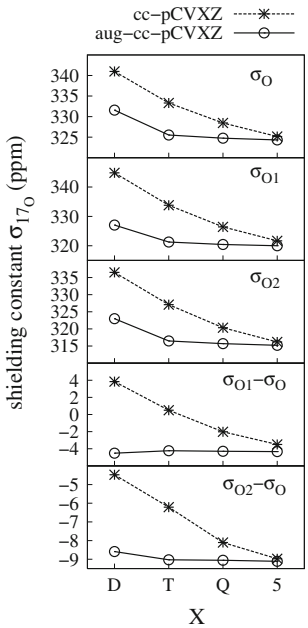

Fig. 2 Basis-set dependence of ^{17}O shielding constants in the water monomer (O) as well as donor (O1) and acceptor (O2) molecules of the water dimer, and the change from monomer to donor/acceptor in the dimer as a function of basis-set quality. B3LYP calculations are shown

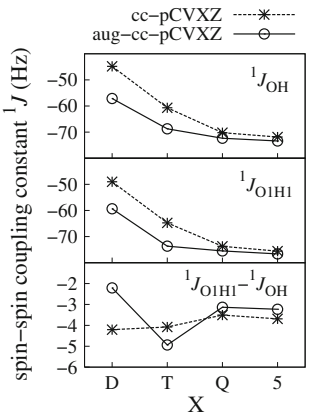

Fig. 3 Basis-set dependence of $^1J_{O1H1}$ spin–spin coupling constants for monomer (OH), dimer (O1H1), and their difference. The hydrogen atom H1 participates in the hydrogen bond. B3LYP calculations are shown

interaction-induced effect on NMR parameters. It turns out that the aug-cc-pCVTZ basis performs well in all cases other than the $^1J_{O1H1}$ spin–spin coupling constant, which would require the quadruple zeta level, as can be seen in the bottom part of Fig. 3. Regarding the overall performance and computational cost, aug-cc-pCVTZ appears to be a good choice for production calculations, keeping in mind the nice performance with shieldings and NQCCs but only a restricted validity when the spin–spin coupling is concerned.

Other studies have found the performance of the DFT/B3LYP level of theory suitable for qualitative NMR calculations of water using aug-cc-pVDZ for shieldings [48] and a triple-zeta basis set supplemented with tight functions for spin–spin couplings [49]. Kongsted et al. [25] found that the DFT error for the acceptor oxygen shielding constant as a function of dimer geometry differs between the different DFT functionals, as referenced to high-level CCSD(T) results. Table 1 compares the present DFT, Hartree-Fock and coupled-cluster calculations to the literature data for both the monomer and the dimer, both at their equilibrium geometry.

The results reveal that the performance of B3LYP is no inferior to that of the recommended [25] KT3 functional [57] when all NMR parameters are compared against the CC reference or, in the monomer case, to experiment. Small differences should have no effect on overall conclusions based on the present B3LYP results. B3LYP shows a reasonable overall performance with respect to the present CC data, as well as recent high-level calculations, thus validating the choice of this functional for the production calculations. The significance of the DFT errors is diminished by the fact that the present work concentrates on the trends occurring in the property surfaces of the dimer, which are obtained as differences between the dimer and monomer values. These trends are only slightly affected by the systematic errors of the method.

One might question the applicability of DFT for relatively weak interactions taking place between molecules. Whereas accurate intermolecular interaction energies typically require using correlated ab initio methods, the corresponding effects on NMR parameters, determined by one-electron operators sampling a region of space weighed heavily to the proximity of nuclei, are seen to be rather well reproduced at the DFT level. In the case of water dimer, the electrostatic and monomer overlap effects play key roles in the NMR property surfaces, and both can be expected to be captured reasonably by DFT. In fact, even in the case of a xenon dimer, where the energetics obtains a major dispersion contribution, already the Hartree-Fock theory is able to convey the qualitative features of inter-atomic NMR property surfaces [58, 59].

3.1.2 *Basis-set superposition error tests*

The importance of basis-set superposition error (BSSE) effects [60] was tested using the counterpoise (CP) correction scheme of Boys and Bernardi [61], modified to include changes in the monomer geometry [62]. The ratio of the CP correction term to the uncorrected interaction-induced change is displayed in Table 2 for each NMR parameter of the water dimer at $R_{OO} = 2.9$ Å and $\alpha = 0°$ geometry. The conclusion is that BSSE needs not to be corrected for in the cases of nuclear shielding, shielding anisotropy, or NQCC with the presently used combination of method and basis set. These properties may indicate large relative BSSE in some specific cases but this behaviour can be traced back to the small magnitude of the interaction-induced change, causing any correction to appear large in the relative sense. On the contrary, spin–spin couplings show significant BSSE effects up to more than 40% for OH couplings of the donor molecule and up to 10% for the acceptor. In production calculations, we decide not to correct for BSSE, keeping in mind the possible consequences for spin–spin couplings.

We note that Kongsted et al. [25] also obtained quite small BSSE effects on shielding in their study of $(H_2O)_2$ using the aug-cc-pVTZ basis set. In the same context, already Chesnut and Rusiloski [21] mention the little need of performing CP corrections for the water dimer when basis sets containing diffuse functions are employed.

3.2 Production calculations

3.2.1 *Geometry and potential energy*

The optimised dimer geometry at the B3LYP/aug-cc-pVTZ level has $R_{OO} = 2.917$ Å and $\alpha = 5.30°$. The former value

Table 1 Calculated NMR properties of water monomer and dimer at different levels of theory

	B3LYP	KT3	HF[b]	CC[c]	Literature
Monomer[a]					
σ_O	325.5	325.0	326.6	336.3	325.3[d]
σ_H	31.08	31.40	30.52	30.79	30.05[e]
$\Delta\sigma_O$	54.7	50.7	56.5	49.1	46.9[f]
$\Delta\sigma_H$	19.16	18.61	20.35	19.92	19.08[f]
χ_O	10.38	11.06	10.63	9.78	10.11[g]
χ_D	0.322	0.314	0.321	0.329	0.308[h]
$^1J_{OH}$	−68.7	−71.1	–	−73.7	−78.7[i], −80.6[j]
$^2J_{HH}$	−5.58	−8.86	–	−6.81	−7.34[j]
Dimer[k]					
σ_{O1}	−4.2	−3.4	−0.8	−3.6	−3.4[l], −1.3[m]
σ_{O2}	−9.0	−8.5	−6.5	−7.1	−7.3[l], −5.6[m]
σ_{H1}	−3.13	−3.04	−3.13	−2.99	−2.94[l], −2.45[m]
σ_{H2}	0.40	0.40	0.48	0.37	0.36[n]
σ_{H3}	−0.65	−0.67	−0.58	−0.61	−0.48[n]
$\Delta\sigma_{O1}$	11.5	11.7	7.7	10.1	8.5[o]
$\Delta\sigma_{O2}$	−12.5	−10.8	−11.4	−10.8	
$\Delta\sigma_{H1}$	11.13	10.90	10.82	10.90	12.03[o]
$\Delta\sigma_{H2}$	−0.08	0.01	0.04	−0.04	0.38[o], 0.0[p]
$\Delta\sigma_{H3}$	−0.27	−0.25	−0.13	−0.19	−0.6[p]
χ_{O1}	−0.78	−0.78	−0.75	−0.70	
χ_{O2}	−0.25	−0.30	−0.19	−0.22	
χ_{D1}	−0.041	−0.040	−0.043	−0.041	
χ_{D2}	0.004	0.004	0.005	0.004	
χ_{D3}	−0.005	−0.005	−0.005	−0.005	
$^1J_{O1H1}$	−4.9	−4.6	–	−4.0	−4.5[q], −7.3[r]
$^1J_{O1H2}$	−1.6	−1.8	–	−1.1	−0.7[q], −2.7[r]
$^2J_{H1H2}$	0.22	0.49	–	0.30	−0.14[q], −0.35[r]
$^1J_{O2H3}$	−3.4	−3.6	–	−2.6	−2.4[q], −4.5[r]
$^2J_{H3H4}$	−0.03	0.04	–	1.75	−0.1[q], −0.4[r]

DFT results using the B3LYP and KT3 functionals, as well Hartree-Fock (HF) and coupled-cluster (CC) data are shown for the shielding constants (σ, in ppm), shielding anisotropies ($\Delta\sigma$, ppm), quadrupole couplings (χ, MHz) and spin–spin couplings (J, Hz). For the dimer, changes with respect to the monomer values are given

[a] Unless otherwise indicated, present calculations using the aug-cc-pCVTZ basis set and the optimised (at the B3LYP/aug-cc-pVTZ level) monomer ($r_{OH} = 0.9618$ Å, $\angle H - O - H = 105.09°$) and dimer ($R_{OO} = 2.9173$ Å, $\alpha = 5.30°$) geometries

[b] Spin–spin couplings not calculated at the HF level

[c] $\sigma, \Delta\sigma$ and χ with CCSD(T), J with CCSD

[d] Analysis of experimental spin-rotation data in Ref. [50]. Best estimate of the equilibrium geometry value 337.7 ppm is obtained by subtracting the computed rovibrational contribution [50]

[e] Analysis of experimental gas-phase data in Ref. [51]. An estimate of the equilibrium geometry value 30.6 ppm is obtained by subtracting the computed rovibrational contribution −0.55 ppm at 300 K [14] from the experimental value

[f] MCSCF calculation including rovibrational contributions at 300 K of −2.4 and −1.08 ppm for ^{17}O (in $^1H_2^{17}O$) and ^1H (in $^1H_2^{16}O$), respectively [14]. The equilibrium geometry values are 49.3 and 20.16 ppm for ^{17}O and ^1H, respectively

[g] Microwave experiment [52]. An estimate of the equilibrium geometry value 9.93 MHz is obtained by subtracting the computed rovibrational contribution 0.18 MHz at 298 K [16] from the experimental value

[h] Molecular beam experiment [53]. An estimate of the equilibrium geometry value 0.312 MHz is obtained by subtracting the computed rovibrational contribution −0.004 MHz at 298 K [16] from the experimental value

[i] NMR measurement in cyclohexane-d_{12} solution at 293 K [54]. An estimate of the equilibrium geometry value −83.0 Hz is obtained by subtracting the computed rovibrational contribution 4.34 Hz at 300 K [15] from the experimental value

[j] NMR measurement in CD_3NO_2 solution at 323 K ($^1J_{OH}$) and 297 K ($^2J_{HH}$) [55]. Estimates of the equilibrium geometry values −85.0/−7.9 Hz are obtained by subtracting the computed rovibrational contributions 4.39/0.55 Hz at 340/300 K [15] from the experimental values of $^1J_{OH}/^2J_{HH}$

[k] For the dimer, the changes in the parameters with respect to the monomer values, a(dim) − a(mon), are indicated. Only one result (H3/D3) for the acceptor hydrogens is displayed because the hydrogens have symmetric positions at the equilibrium geometry

[l] Ref. [25]. CCSD(T)/aug-cc-pVTZ level of theory, at the dimer geometry optimised at the same level

[m] Ref. [23]. CCSD/aug-cc-pVTZ level of theory, at the experimental dimer geometry [8]

[n] Ref. [21]. HF/6-311++G(2d,2p) level of theory, at the experimental dimer geometry

[o] Ref. [20]. HF/4-31G level of theory

[p] Ref. [56]. HF calculation

[q] Ref. [22]. RASSCF(RAS1)/HIIIa level of theory, at the experimental dimer geometry [8]

[r] Ref. [22]. As in footnote *q* but with the dimer immersed in a dielectric continuum model simulating liquid water

Table 2 Basis set superposition errors estimated with the modified counterpoise method [62] at the B3LYP/aug-cc-pCVTZ level for the near-equilibrium dimer geometry $R_{OO} = 2.9$ Å and $\alpha = 0°$

A[a]	A(dim) − A(mon)	$BSSE_{absolute}$	$BSSE_{\%}$	[A(dim) − A(mon)]$_{CP}$
σ_{O1}	−4.73	−0.04	−0.92	−4.77
σ_{O2}	−9.10	0.06	0.62	−9.04
σ_{H1}	−3.22	−0.01	−0.22	−3.23
$\Delta\sigma_{O1}$	9.53	−0.08	−0.83	9.47
$\Delta\sigma_{O2}$	−13.12	−0.02	−0.19	−13.12
$\Delta\sigma_{H1}$	11.51	0.01	0.07	11.52
χ_{O1}	−0.82	0.00	−0.17	−0.82
χ_{O2}	−0.25	−0.01	−2.34	−0.25
χ_{D1}	−0.041	0.000	0.38	−0.041
$^1J_{O1H1}$	−5.05	2.24	44.33	−2.81
$^1J_{O2H3}$	−3.75	0.38	10.03	−3.38

Results with and without the BSSE, as well as the absolute and relative BSSE are displayed

[a] Shielding constants and anisotropies in ppm, quadrupole couplings in MHz, and spin–spin couplings in Hz

resides within the rather large error margins of the experimental result by Dyke [9], $R_{OO} = 2.98 \pm 0.33$ Å. Klopper et al. [11] obtained in their benchmark CCSD(T) calculations $R_{OO} = 2.912 \pm 0.005$ Å and $\alpha = 5.5°$. Consequently, the present B3LYP/aug-cc-pVTZ geometry agrees extremely well with the best existing estimate.

During each point of the restricted geometry optimisation, the dimer parameters R_{OO} and α are not allowed to change while the rest of the geometry relaxes. The overall appearance of the dimer after optimisation is quite different for small α angles when compared with large angles. Figure 4 illustrates the gradual changes. With moderate α (0°–15°), the orientation of the monomers with respect to each other in the dimer closely resembles that of the global equilibrium geometry [11]. The hydrogen bond angle is not restricted to lie in the symmetry plane of the dimer, however. As α increases further (20°–30°), monomer orientations gradually evolve, finally (35°–45°) ending up into a situation, where the distinction of the donor and the acceptor molecules has disappeared. At this point, the hydrogen bond angle α equals 45°. Because the molecules are in symmetric positions with respect to one another, also the other angle α', the equivalent of α with the roles of the donor and acceptor interchanged, is also 45°. If the angle α is increased over 45°, the donor and acceptor labels swap, and α' takes the role of α as the hydrogen bond angle. In vibration-rotation-tunnelling spectroscopy, this type of process is called "donor-acceptor-interchange" and it is one of the tunnelling processes in the water dimer [63, 64]. The sequence of geometries in a restricted geometry optimisation of the water dimer as the hydrogen bond angle gradually increases resembles the rearrangement pathway for the donor-acceptor-interchange tunnelling, the hydrogen bond angle being the reaction coordinate. Thus, the symmetric geometry where both α and α' equal 45° can be seen as a transition state.

Figure 5 shows the variation of the covalent bond lengths and intramolecular angles of the donor and acceptor as a function of R_{OO} and α. The covalent O1H1 bond directly involved in the hydrogen bond elongates upon dimerisation, with the elongation amounting to less than 0.01 Å and being most noticeable near the equilibrium

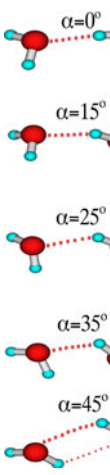

Fig. 4 Changes in the overall dimer geometry as the hydrogen bond angle α changes from 0° to 45°

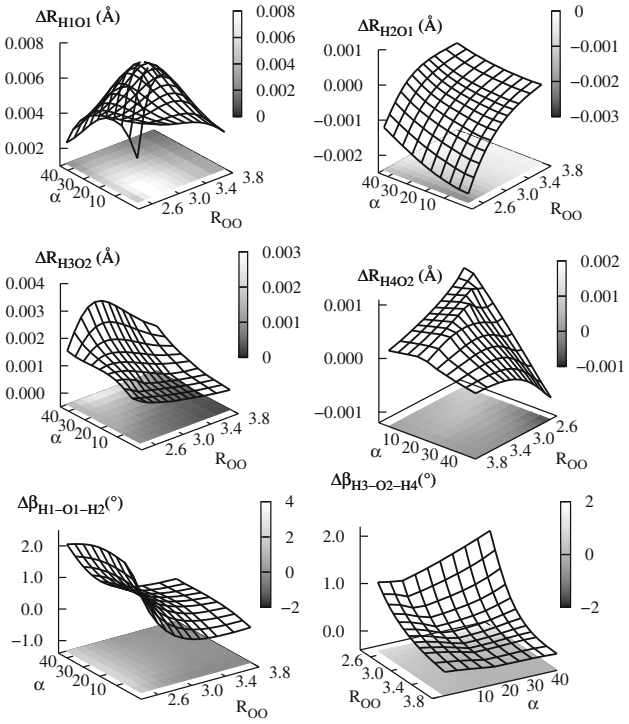

Fig. 5 Variation of the donor and acceptor bond lengths and angles in water dimer as a function of the intermolecular oxygen–oxygen distance R_{OO} and hydrogen bond angle α. B3LYP/aug-cc-pVTZ level of theory

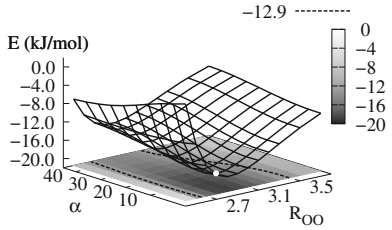

Fig. 6 B3LYP/aug-cc-pCVTZ potential energy surface of the water dimer as a function of the intermolecular oxygen–oxygen distance R_{OO} and hydrogen bond angle α. The *marked point* indicates the equilibrium geometry and the *black projected curve* is an equipotential contour corresponding to the value at the point $R_{OO} = 3.5$ Å and $\alpha = 0°$.

geometry. The other covalent bonds are considerably less affected. As the monomers approach each other, the bond angles of both the acceptor and the donor remain close to the free monomer value all the way down to the equilibrium distance of the dimer. An even closer encounter makes both angles open up by a couple of degrees.

The potential energy surface of the dimer is illustrated in Fig. 6. The energy surface has a repulsive core region at small R_{OO} values and approaches zero for large R_{OO}. As a function of α the changes are modest. Around the equilibrium value of R_{OO} at about 2.9 Å, the energy landscape has a valley as α traverses its range, indicating the rearrangement pathway for the donor-acceptor-interchange tunnelling. The potential energy at the equilibrium geometry is about −19 kJ/mol and the energy of the transition state is about 4.4 kJ/mol higher, with no corrections applied for basis-set superposition error.

3.2.2 *Property surfaces*

Table 1 points out the major changes caused by hydrogen bonding on the NMR parameters of the water dimer at the equilibrium geometry. They occur in the nuclei that are directly involved in the O2···H1–O1 bond. Among their parameters, the most dramatic effects occur for the anisotropy of the acceptor and donor oxygens, $\Delta\sigma_{O2}$ and $\Delta\sigma_{O1}$, which undergo a 20% (10 ppm) decrease and increase, respectively, as well as $\Delta\sigma_{H1}$ that increases by 50% from its monomer value to ca. 30 ppm. Large changes in the shielding constant and anisotropy of H1 with $R_{OO} < 3.5$ Å were already found by Ditchfield [20], who also pointed out that the anisotropy may be more indicative of hydrogen bonding than changes in the isotropic shielding constants. In a similar vein, the NQCC of D1 decreases by roughly 40 kHz upon dimer formation. The other parameters change relatively little, with a characteristic decrease taking place in the shielding constants (apart from the small increase in the case of the non-bonded donor

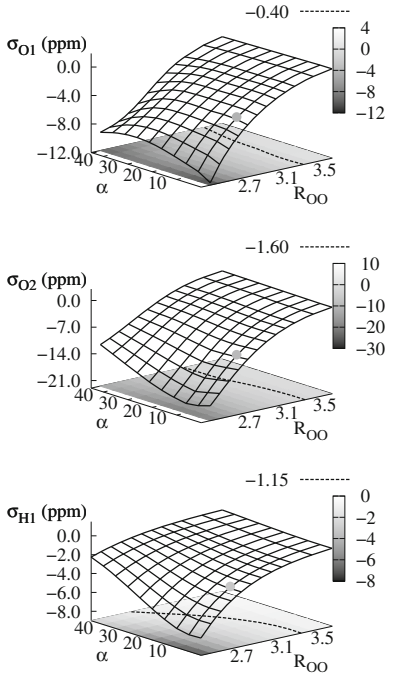

Fig. 7 As Fig. 6 but for the nuclear shielding constant of the water dimer for the donor oxygen O1, acceptor oxygen O2, and hydrogen-bonded hydrogen H1

hydrogen, H2), as well as the one- and two-bond spin–spin couplings.

Figures 7, 8, 9 and 10 show the dimer property surfaces for some of the shielding constants, shielding anisotropies, NQCCs, and intramolecular spin–spin coupling constants, respectively, computed as differences with respect to the corresponding monomer values. Small but representative set of test calculations confirm that the general trends and overall behaviour is similar between B3LYP vs. CCSD(T) for shieldings and B3LYP vs. CCSD for J couplings. Thus, general conclusions based on the B3LYP property surfaces should be reliable.

The depicted surfaces have their maxima (in the absolute sense) usually near ($R_{OO} = 2.5$ Å, $\alpha = 0°$) because at small intermolecular distance the repulsive intermolecular interaction strongly affects the properties. The effect of the neighbouring molecule diminishes smoothly as the intermolecular separation increases. While all the parameters are clearly dependent on R_{OO}, the dependence on the hydrogen bond angle α varies. This can in some cases be traced back to the dependence on the distance between the nucleus or nuclei in question and the closest atom in the neighbouring molecule. For the donor oxygen nucleus (O1), the distance to the closest atom in the acceptor, the oxygen O2, is not changing as α changes in the constrained geometry optimisation. Consequently, the effect of α on σ_{O1} and $\Delta\sigma_{O1}$ is modest. For O2 and H1, the nuclei that are directly involved in the hydrogen bonding, there is a more

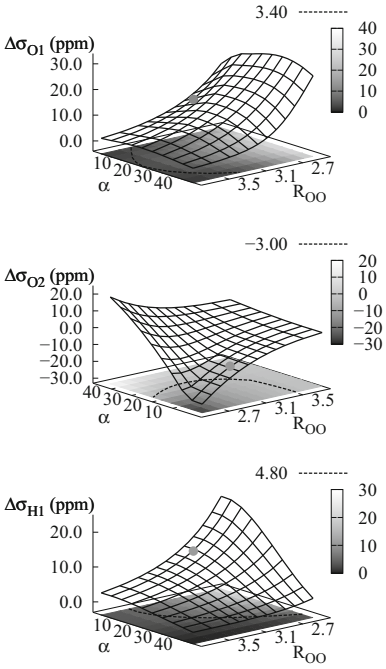

Fig. 8 As Fig. 6 but for the nuclear shielding anisotropy of the water dimer for the donor oxygen O1, acceptor oxygen O2, and hydrogen-bonded hydrogen H1

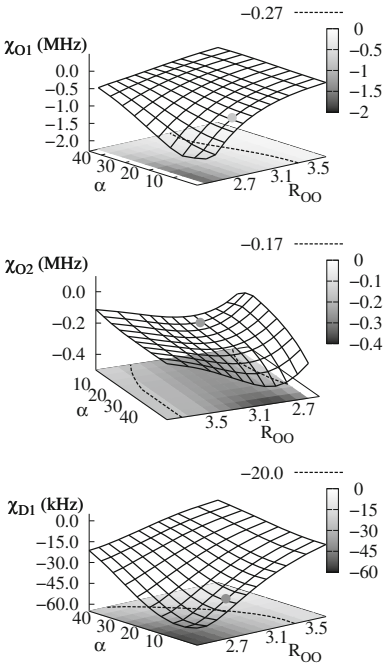

Fig. 9 As Fig. 6 but for the nuclear quadrupole coupling of the water dimer for the donor oxygen O1, acceptor oxygen O2, and hydrogen-bonded deuterium D1

pronounced dependence on α in the shielding constant and anisotropy. The distance between the hydrogen-bonded hydrogen H1 and the acceptor oxygen O2, nearest

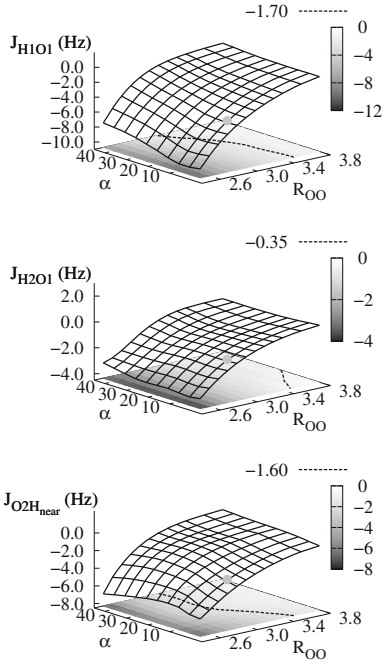

Fig. 10 As Fig. 6 but for the nuclear spin–spin coupling constant surfaces of the water dimer for $^1J_{H1O1}$, $^1J_{H2O1}$, and $^1J_{O2Hnear}$, where H_{near} denotes the hydrogen nucleus of the acceptor which is closest to the donor molecule

neighbours for each other, depends on α, and so do most of the parameters of these nuclei. $\Delta\sigma_{O2}$ even changes to have a positive sign in the depicted portion of the surface, at large α values.

While the shielding anisotropies have a noticeable α-dependence for all the observed nuclei, in general the investigated spin–spin couplings are mostly dependent only on the R_{OO} distance, with little curvature of the surfaces in the direction of changing α. The NQCCs of O1, O2, and D1 are all non-negligibly dependent on the hydrogen bond angle, although the range of overall alteration is small for the acceptor oxygen. We also checked the dimerisation effects on the direction of the principal axis 3, the reference direction for the shielding anisotropy σ_{33}, and observed that its direction tends to turn towards the neighbour. These directional changes are modest for hydrogen-bonded hydrogen H1 and donor oxygen O1, and very small for acceptor oxygen O2.

3.2.3 *Direct interaction effect and indirect geometric effect*

The effect of dimerisation on the NMR properties is analysed further by dividing it into two contributions. On the one hand, the *direct* effect focuses on the intermolecular influence on the properties at a fixed geometry. On the other hand, the *indirect* effect is caused by the dimerisation-induced geometry change of the monomers [29].

However, this often-considered separation is somewhat artificial and contains an ambiguity as demonstrated by the data in Table 3 and the following consideration.

The break-down of the total dimerisation effect into direct and geometric contributions can be realised by using one of two intermediate states that manifest either the former or the latter part, but not both at the same time. If we start with a monomer in its equilibrium geometry, and as a first step transform it into a monomer in a geometry that it assumes in a dimer, we take the upper route with the intermediate state 1 in Table 3. In the second step, the neighbour molecule is introduced and we end up at an interacting dimer at the dimer geometry. The geometric and direct effects on properties can be computed as the changes in the two steps. The other possible choice is to first introduce the neighbour molecule without allowing the geometry of the monomers to change (state 2 in the Table) and only subsequently letting the geometry relax. In principle, the two choices result in distinct analyses into the direct and indirect contributions. It is emphasised that neither of the two paths joining the monomer and dimer situations are physically realised as such; they only serve as a means of analysing the total interaction effect. We use both approaches, and the results are gathered in Table 3.

In eight out of twelve cases, the direct effect is larger than the indirect geometric effect by about a factor of 10 or more. Properties related to the acceptor oxygen O2 change primarily through the direct effect because the geometry changes of the acceptor molecule are modest. Also the dimerisation effects on the shielding anisotropies $\Delta\sigma_{O1}$ and $\Delta\sigma_{H1}$ as well as the quadrupole coupling χ_{O1} arise chiefly due to the direct interaction. In the remaining cases, the absolute magnitude of the geometric effect constitutes more than 10% of the total effect and may reach as much as 40%, which is the case for both the donor oxygen shielding σ_{O1} and the quadrupole coupling of deuterium D1 directly involved in the hydrogen bond. These are the two centres that form the covalent bond that undergoes the largest changes upon dimerisation. The dimerisation-induced changes in the spin–spin couplings $^1J_{O1H1}$ and $^1J_{O1H2}$ of the donor molecule also bear considerable geometric contributions. While the direct and geometric effects occur mostly in the same direction, they may be opposite as well, notably in $^1J_{O1H1}$.

To demonstrate the fundamental ambiguity in the present type of analysis, we also tested the influence on the results of the order in which the geometric and direct effects are applied. Selecting either route one or two in Table 3 is an important factor only for the shielding constant of the donor oxygen, where the two approaches give a notably different partition into geometric and direct contributions. In all the other cases, the order is unimportant. Again, as the O1–H1 covalent bond length is the one that

Table 3 Comparison of the direct intermolecular interaction effect and the indirect geometric effect in the NMR parameters of the water dimer

	mon	Δgeom(1)	state(1)	Δdirect(1)	dim
		Δdirect(2)	state(2)	Δgeom(2)	
σ_{O1} (ppm)	325.5	-1.9 -2.9	323.6 -4.2 322.6	-2.3 -1.3	321.3
σ_{O2} (ppm)	325.5	-0.4 -8.6	325.1 -9.0 316.9	-8.6 -0.4	316.5
σ_{H1} (ppm)	31.08	-0.29 -2.77	30.79 -3.13 28.32	-2.84 -0.36	27.96
$\Delta\sigma_{O1}$ (ppm)	54.7	0.3 11.0	55.0 11.5 65.7	11.2 0.5	66.2
$\Delta\sigma_{O2}$ (ppm)	54.7	0.1 -12.6	54.8 -12.5 42.1	-12.6 0.1	42.2
$\Delta\sigma_{H1}$ (ppm)	19.16	-0.33 11.28	18.83 11.13 30.44	11.46 -0.14	30.29
χ_{O1} (MHz)	10.38	0.04 -0.80	10.42 -0.78 9.58	-0.82 0.02	9.60
χ_{O2} (MHz)	10.38	-0.00 -0.25	10.37 -0.25 10.13	-0.25 -0.00	10.12
χ_{D1} (MHz)	0.322	-0.017 -0.024	0.305 -0.041 0.298	-0.024 -0.017	0.281
$^1J_{O1H1}$ (Hz)	-68.7	1.7 -6.5	-67.0 -4.9 -75.2	-6.6 1.6	-73.7
$^1J_{O1H2}$ (Hz)	-68.7	-0.4 -1.2	-69.1 -1.6 -69.9	-1.2 -0.5	-70.4
$^1J_{O2H3}$ (Hz)	-68.7	-0.3 -3.1	-70.0 -3.4 -71.8	-3.1 -0.3	-72.1

The diagram shows the different partitions into direct and geometric effects obtained using two auxiliary intermediate states (see text for details)

clearly changes in dimerisation, the operations of geometry change and the introduction of the neighbour are not independent in this case, in contrast to the other parameters where they appear additive to a good approximation.

The discussion above suggests that the pairwise additive approximation (PAA) that has been found valid, e.g., for the shielding constant σ_{Xe} in monoatomic xenon gas [65] may not be a sensible one for σ_O in liquid water. In this approximation, it is assumed that each contribution from the neighbouring atoms can be separately evaluated and

accumulated, and that the investigated molecule does not have to be allowed to relax geometrically after adding each neighbour, since the indirect effect can be added afterwards if necessary. The latter condition fails if the geometry change and the addition of the neighbour are not independent operations. For comparison, while the NQCC of the deuterium directly involved in the hydrogen bond obtains a large geometric contribution, the order of the two mentioned operations is not important. Indeed, PAA has been demonstrated to be a good approximation for quadrupole couplings in liquid water [19].

In cases where the pairwise additive approximation holds, the present intermolecular property surfaces may provide a powerful avenue for evaluating the NMR parameters of bulk and surface water, without resorting to expensive, explicit quantum-chemical supermolecule calculations of simulation snapshots. The surface data can be fitted to a suitable functional form, an NMR force field [66], which can be used to calculate the parameters based on the instantaneous position information alone.

3.2.4 *Property surfaces and hydrogen bonding*

The NMR parameters are sensitive to the details of the electronic structure near the resonant nucleus. Interaction with neighbouring molecules changes the electronic structure and thus affects the NMR parameters. The other way around, the changes in the NMR parameters could in principle be used to identify the neighbours of the molecule, e.g., to judge whether the molecule is involved in a hydrogen bond. Based on the computed property surfaces for the water dimer, we may try to identify a useful definition of a hydrogen bond that exploits the changes in the NMR parameters caused by dimerisation. Such definitions are typically expressed geometrically.

In the present data, the dimer parameters approach those of an isolated water molecule at a large separation of the monomers. Utilising this tendency, a suitable cut-off distance criterion can be selected that determines when the dimer parameter deviates enough from the corresponding monomer parameter, to be considered as having a strong interaction with its neighbour. A general feature of all the present NMR parameter surfaces is that they are smooth, revealing no abrupt changes, as well as well converged to the monomer values as a function of distance within our range of intermolecular geometries. Even the somewhat more strict, commonly used cut-off distance of about 3.5 Å can on the basis of our data be used to define an approximate range where the interaction appreciably affects the NMR parameters. In contrast, the interaction energy seems not be converged at this distance.

For the angle α, there cannot be an NMR-based, generally applicable cut-off value that would be independent of R_{OO}. This is due to the fact that some nuclei, especially the hydrogen-bonded centre H1 turns away from the acceptor molecule with increasing α, eventually becoming effectively free. At the same time, the oxygens stay at a separation R_{OO}, with the consequence that their NMR parameters continue to be affected regardless of the angle. Hence, the oxygens do not become free as α increases. This means that there cannot be any generally valid range of α for hydrogen bonding that would be defined through changes in NMR parameters when compared to the monomer. However, if α increases without limit, the hydrogen atom H1 no longer stays in between the two molecules and eventually ceases to participate in hydrogen bonding. Consequently, we must from this purely geometric point-of-view restrict α, and the natural upper limit for α equals 45° because at this point the restricted geometry optimisation pushes the dimer into a geometry where two hydrogen bonds coexist, as depicted in Fig. 4.

Summarising, a hydrogen bond definition that is compatible with the NMR data can be expressed as $R_{OO} \leq 3.5$ Å and $\alpha(\mathrm{H1–O1\cdots O2}) \leq 45°$. For comparison, the geometric "strong" hydrogen bond criterion of Mezei and Beveridge [26] ($R_{OO} \leq 3.3$ Å and $\alpha \leq 45°$) and the definition of Luzar and Chandler [27] ($R_{OO} \leq 3.5$ Å and $\alpha \leq 30°$) are in a good agreement with the present suggestion. A very recent discussion about the different definitions can be found in the article by Kumar, Schmidt and Skinner [28]. Comparison with techniques other than NMR shows, e.g., that the range of the first coordination shell in liquid water as determined experimentally from the oxygen–oxygen radial distribution function, is about 3.5 Å [37], which indicates the range of the hydrogen bonding interaction. The use of NMR parameters to identify hydrogen bonding complements and reinforces the validity of the widely used hydrogen bond definitions. Our findings are in unison with the traditional notion of the hydrogen bond, and the overall smoothness of the NMR property surfaces prevents us from giving any novel definition.

4 Conclusions

We have monitored the changes in the NMR parameters of the water dimer, calculated at the DFT/B3LYP/aug-cc-pCVTZ level of theory, as functions of two intermolecular coordinates, the oxygen–oxygen distance R_{OO} and the hydrogen bond angle $\alpha = \angle(\mathrm{H1-O1\cdots O2})$. The studied parameters are the nuclear shielding constants, shielding anisotropies, and quadrupole coupling constants, as well as the intramolecular spin–spin coupling constants.

The behaviour of the intramolecular geometry, interaction energy, and NMR parameters was illustrated as property surfaces where the changes induced by dimerisation are

seen as functions of R_{OO} and α, with all the other intra- and intermolecular geometric variables optimised. The dimerisation mainly affects the parameters of the donor and acceptor oxygens as well as the hydrogen centre H1. Particularly, the shielding anisotropies of these nuclei, as well as the quadrupole coupling constant of the deuterium directly involved in the hydrogen bond, undergo large changes upon dimerisation. In general, smooth property surfaces are obtained for all the parameters, indicating no abrupt changes on the (R_{OO}, α) surface. The dependence on the R_{OO} distance is mostly a monotonic decay to the monomer value of the parameter at large R_{OO}, with the only exception constituted by the quadrupole coupling of the acceptor oxygen, which features a saddle surface. The dependence on α is generally weaker and more varied than that on R_{OO}.

Analysis of the total dimerisation influence on the main NMR parameters was performed in terms of the contributions from an indirect effect via the geometry change and direct intermolecular effect at fixed geometry. The direct interaction effect is found to always dominate the total change, but the indirect influence should generally be included as well. It is shown, however, that this analysis is not unique, in the sense that the operations of relaxing to the dimer geometry and introducing the neighbouring molecule are generally not additive. This manifests itself by a different partitioning of the total interaction effect into the indirect and direct contributions, depending on the order in which the two steps are taken. In practice, of the currently investigated NMR properties of the water dimer, only the nuclear shielding constant of the donor oxygen is significantly affected by this. For parameters such as this, approximating the total intermolecular interaction effect in terms of pairwise additive intermolecular contributions may not be valid.

Pairwise additivity justifies the use of a preparameterised NMR force field, obtainable from fitting a suitable model function to our property surfaces. Such a parametrisation would enable efficient calculation of the NMR parameters of differently coordinated water molecules in the bulk and at surfaces, based on coordinate data alone.

Analysis of the NMR property surfaces can be attempted with the purpose of obtaining an NMR-based hydrogen bond definition expressed in terms of R_{OO} and α. Due to the smoothness of the property surfaces, the analysis is not capable of producing fundamentally new insight into the applicable geometric definitions. Our result, $R_{OO} \leq 3.5$ Å and $\alpha \leq 45°$, coincides with the widely used definitions.

Acknowledgments TP is grateful to the financial support from the Graduate School of Computational Chemistry and Molecular Spectroscopy, Oulu University Scholarship Foundation, Research Foundation of Orion Corporation, The Finnish Foundation for Economic and Technology Sciences—KAUTE, Magnus Ehrnrooth Foundation, and Finnish Cultural Foundation. The authors belong to the Finnish Center of Excellence in Computational Molecular Science (CMS, 2006-11). PL is Academy Research Fellow of the Academy of Finland. Computational resources were partially provided by CSC—Scientific Computing Ltd, Espoo, Finland.

References

1. Wernet Ph, Nordlund D, Bergmann U, Cavalleri M, Odelius M, Ogasawara H, Näslund LÅ, Hirsch TK, Ojamäe L, Glatzel P, Pettersson LGM, Nilsson A (2004) Science 304:995–1012
2. Stillinger FH (1980) Science 209:451
3. Eisenberg D, Kauzmann W (1969) The structure and properties of water. Clarendon, Oxford
4. Prendergast D, Galli G (2006) Phys Rev Lett 96:215502
5. Wang RLC, Kreuzer HJ, Grunze M (2006) Phys Chem Chem Phys 8:4744
6. Soper AK (2005) J Phys Condens Matter 17:S3273
7. Bukowski R, Szalewicz K, Groenenboom GC, van der Avoird A (2007) Science 315:1249
8. Odutola JA, Dyke TR (1980) J Chem Phys 72:5062
9. Dyke TR (1984) Top Curr Chem 120:85
10. Halkier A, Koch H, Jørgensen P, Christiansen O, Nielsen IMB, Helgaker T (1997) Theor Chem Acc 97:150
11. Klopper W, van Duijneveldt-van de Rijdt JGCM, van Duijneveldt FB (2000) Phys Chem Chem Phys 2:2227
12. Hakala M, Nygård K, Manninen S, Huotari S, Buslaps T, Nilsson A, Pettersson LGM, Hämäläinen K (2006) J Chem Phys 125:084504
13. Levitt MH (2001) Spin dynamics: basics of nuclear magnetic resonance. Wiley, Chichester
14. Vaara J, Lounila J, Ruud K, Helgaker T (1998) J Chem Phys 109:8388
15. Wigglesworth RD, Raynes WT, Sauer SPA, Oddershede J (1998) Mol Phys 94:851
16. Olsen L, Christiansen O, Hemmingsen L, Sauer SPA, Mikkelsen KV (2002) J Chem Phys 116:1424
17. Pennanen TS, Vaara J, Lantto P, Sillanpää AJ, Laasonen K, Jokisaari J (2004) J Am Chem Soc 126:11093, and references therein
18. Pennanen TS, Lantto P, Sillanpää AJ, Vaara J (2007) J Phys Chem A 111:182
19. Müller MG, Kirchner B, Vogt PS, Huber H, Searles DJ (2001) Chem Phys Lett 346:160
20. Ditchfield R (1976) J Chem Phys 65:3123
21. Chesnut DB, Rusiloski BE (1993) J Phys Chem 97:2839
22. Pecul M, Sadlej J (1999) Chem Phys Lett 308:486
23. Pecul M, Lewandowski J, Sadlej J (2001) Chem Phys Lett 333:139
24. Pecul M, Sadlej J, Helgaker T (2003) Chem Phys Lett 372:476
25. Kongsted J, Aidas K, Mikkelsen KV, Sauer SPA (2008) J Chem Theory Comput 4:267
26. Mezei M, Beveridge DL (1981) J Chem Phys 74:622
27. Luzar A, Chandler D (1996) Phys Rev Lett 76:928
28. Kumar R, Schmidt JR, Skinner JL (2007) J Chem Phys 126:204107
29. Åstrand P-O, Mikkelsen KV, Ruud K, Helgaker T (1996) J Chem Phys 100:19771
30. Ramsey NF (1950) Phys Rev 78:699
31. Ramsey NF (1953) Phys Rev 91:303
32. Kowalewski J, Mäler L (2006) Nuclear spin relaxation in liquids: theory, experiments, and applications. Taylor & Francis, Boca Raton, FL

33. Abragam A (1961) The principles of nuclear magnetism. Oxford University Press, Oxford
34. Slichter CP (1990) Principles of magnetic resonance, 2nd edn. Springer, Berlin
35. Struis RPWJ, De Bleijser J, Leyte JC (1987) J Phys Chem 91:1639
36. Nygård K, Hakala M, Manninen S, Andrejczuk A, Itou M, Sakurai Y, Pettersson LGM, Hämäläinen K (2006) Phys Rev E 74:031503
37. Sorenson JM, Hura G, Glaeser RM, Head-Gordon T (2000) J Chem Phys 113:9149
38. Becke AD (1993) J Chem Phys 98:5648
39. Stephens PJ, Devlin FJ, Chabalowski CF, Frisch MJ (1994) J Phys Chem 98:11623
40. Frisch MJ, Trucks GW, Schlegel HB, Scuseria GE, Robb MA, Cheeseman JR, Montgomery JA Jr, Vreven T, Kudin KN, Burant JC, Millam JM, Iyengar SS, Tomasi J, Barone V, Mennucci B, Cossi M, Scalmani G, Rega N, Petersson GA, Nakatsuji H, Hada M, Ehara M, Toyota K, Fukuda R, Hasegawa J, Ishida M, Nakajima T, Honda Y, Kitao O, Nakai H, Klene M, Li X, Knox JE, Hratchian HP, Cross JB, Bakken V, Adamo C, Jaramillo J, Gomperts R, Stratmann RE, Yazyev O, Austin AJ, Cammi R, Pomelli C, Ochterski JW, Ayala PY, Morokuma K, Voth GA, Salvador P, Dannenberg JJ, Zakrzewski VG, Dapprich S, Daniels AD, Strain MC, Farkas O, Malick DK, Rabuck AD, Raghavachari K, Foresman JB, Ortiz JV, Cui Q, Baboul AG, Clifford S, Cioslowski J, Stefanov BB, Liu G, Liashenko A, Piskorz P, Komaromi I, Martin RL, Fox DJ, Keith T, Al-Laham MA, Peng CY, Nanayakkara A, Challacombe M, Gill PMW, Johnson B, Chen W, Wong MW, Gonzalez C, Pople JA (2004) Gaussian 03, revision C.02. Gaussian Inc., Wallingford, CT
41. Dunning ThH Jr (1989) J Chem Phys 90:1007
42. Kendall RA, Dunning ThH Jr, Harrison RJ (1992) J Chem Phys 96:6796
43. DALTON, a molecular electronic structure program, release 2.0 (2005) See http://www.kjemi.uio.no/software/dalton/dalton.html
44. Woon DE, Dunning ThH Jr (1995) J Chem Phys 103:4572
45. Stanton JF, Gauss J, Watts JD et al, ACES II Mainz-Austin-Budapest version; see also Stanton JF, Gauss J, Watts JD, Lauderdale WJ, Bartlett RJ (1992) Int J Quantum Chem, Quantum Chem Symp 26:879. Current version, see http://www.aces2.de
46. Wolinski K, Hinton JF, Pulay P (1990) J Am Chem Soc 112:8251
47. Helgaker T, Jørgensen P (1991) J Chem Phys 95:2595
48. Cybulski H, Sadlej J (2006) Chem Phys 323:218
49. Peralta JE, Scuseria GE, Cheeseman JR, Frisch MJ (2003) Chem Phys Lett 375:452
50. Puzzarini C, Cazzoli G, Harding ME, Vázquez J, Gauss J (2009) J Chem Phys 131:234304
51. Raynes WT (1978) Spec Per Reps Nucl Magn Reson 7:1
52. Bellet J, Lafferty WJ, Steenbeckeliers G (1973) J Mol Spectrosc 47:388
53. Garvey RM, DeLucia FC (1988) Can J Phys 55:1115
54. Wasylishen RE, Friedrich JO (1987) Can J Chem 65:2238
55. Sergeyev NM, Sergeyeva ND, Strelenko YA, Raynes WT (1997) Chem Phys Lett 277:142
56. Höller R, Lischka H (1981) Chem Phys Lett 84:94
57. Keal TW, Tozer DJ (2004) J Chem Phys 121:5654
58. Hanni M, Lantto P, Runeberg N, Jokisaari J, Vaara J (2004) J Chem Phys 121:5908
59. Hanni M, Lantto P, Ilias M, Jensen HJAa, Vaara J (2007) J Chem Phys 127:164313
60. van Duijneveldt FB, van Duijneveldt-van de Rijdt JGCM, van Lenthe JH (1994) Chem Rev 94:1873
61. Boys SF, Bernardi F (1970) Mol Phys 19:553
62. Xantheas SS (1996) J Chem Phys 104:8821
63. Dyke TR (1977) J Chem Phys 66:492
64. Watanabe Y, Taketsugufoot T, Wales DJ (2004) J Chem Phys 120:5993
65. Hanni M, Lantto P, Vaara J (2009) Phys Chem Chem Phys 11:2485
66. Vaara J (2007) Phys Chem Chem Phys 9:5399